

Image inpainting for corrupted images by using the semi-super resolution GAN

1st Mehrshad Momen Tayefeh
 dept. Computer Engineering
 Sharif University of Technology
 International Campus
 Kish, Iran
 mehrshadmomen@sharif.edu

2nd Mehrdad Momen Tayefeh
 dept. Electrical and Computer Engineering
 University of Tehran
 Tehran, Iran
 mehrdad.momen@ut.ac.ir

3rd S. AmirAli GH. Ghahramanie
 dept. Computer Engineering
 Sharif University of Technology
 International Campus
 Kish, Iran
 ghahramani@pardis.sharif.edu

Abstract—Image inpainting is a valuable technique for enhancing images that have been corrupted. The primary challenge in this research revolves around the extent of corruption in the input image that the deep learning model must restore. To address this challenge, we introduce a Generative Adversarial Network (GAN) for learning and replicating the missing pixels. Additionally, we have developed a distinct variant of the Super-Resolution GAN (SRGAN), which we refer to as the Semi-SRGAN (SSRGAN). Furthermore, we leveraged three diverse datasets to assess the robustness and accuracy of our proposed model. Our training process involves varying levels of pixel corruption to attain optimal accuracy and generate high-quality images.

Index Terms—Deep learning, GAN, image inpainting

I. Introduction

DEEP learning has revolutionized numerous fields, including classification [1], noise reduction [2], object detection [3], and even channel estimation in wireless communication [4], [5]. One of the pivotal aspects of photo editing resides in the technique of image inpainting, which has undergone significant advancement through the application of deep learning methodologies. Within this domain, a central challenge is the precise reconstruction of missing image segments or pixels or the removal of undesirable elements from photographs while simultaneously reconstructing the background of the edited region. These tools serve a vital purpose in the restoration of aged photographs, striving to closely mirror the original image. Consequently, the utilisation of generative models has proven to be instrumental in achieving the highest level of fidelity in photo restoration. It should be noted that augmenting the extent of damage is an unavoidable consequence of expanding the scope of restoration.

In recent research endeavours, certain authors have ventured into employing statistical approaches for the purpose of hole reconstruction within images. Notably, the PatchMatch algorithm, introduced by the authors of [6], represents a groundbreaking method for establishing nearest-neighbour correspondences between patches in images efficiently. This algorithm has the capacity to facilitate a spectrum of structural image editing tasks, encompassing texture synthesis, image completion, and

image inpainting. Furthermore, the work of Hays et al. [7] addresses the issue of scene completion by harnessing an extensive dataset of photographic images. The authors have introduced a method capable of automatically filling in missing or obscured regions within images by seeking relevant patches within a vast collection of photographic data. Through the selection and seamless integration of patches from this diverse dataset, the algorithm is able to synthesise scene completions that are both coherent and visually plausible.

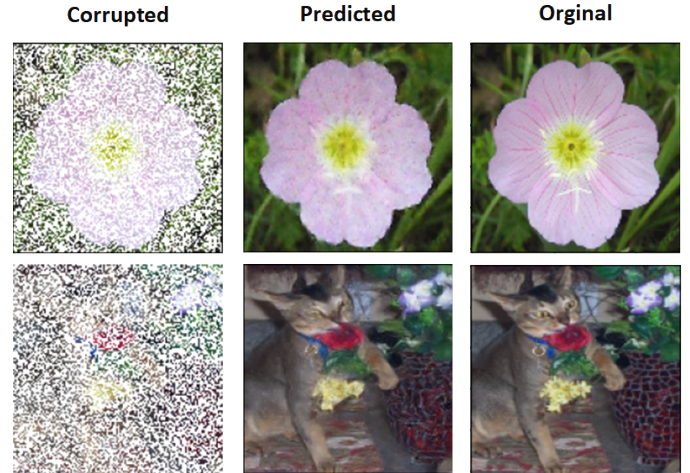


Fig. 1. An instance of reconstructing the missed pixels by using our method.

Conversely, a multitude of methods have emerged by leveraging deep learning approaches to attain the desired output. A substantial body of work, including numerous Convolutional Neural Network (CNN)-based approaches [8], [9], has been proposed for predicting and reconstructing image gaps with notable accuracy. In the work of [10], the authors have presented a novel approach where CNNs acquire meaningful image features through the prediction of missing image components. This methodology employs masked input images and trains the network to restore the masked regions, thereby compelling the network

to discern the intricate context and interdependencies within the image. Additionally, the Generative Adversarial Network (GAN) framework has emerged as a distinct method for image inpainting. GANs, which consist of a generator and discriminator, excel at generating images from noise, rendering them a potent tool for predicting and reconstructing missing image portions. In the work of [11], a patch-based approach is employed within a GAN framework to generate missing content in images by incorporating both local and global contexts. This framework enables the generation of realistic and coherent inpainted regions by training a generator network in an adversarial fashion against a discriminator network. Furthermore, Yu et al. [12] have introduced a generative image inpainting method featuring contextual attention. In this approach, a dual-path generator network is utilized to address both global and local details, with contextual attention mechanisms guiding the network's focus towards pertinent regions for inpainting, thereby enhancing visual coherence. Lastly, in the work of [13], a multi-scale neural patch synthesis approach is presented for high-resolution image inpainting. This method entails generating patches from the surrounding content and training a network to reconstruct the missing regions. The network is designed to synthesize coherent and detailed patches, yielding high-quality image restoration results.

In the context of this research endeavour, we introduce a tailored iteration of the Super-Resolution GAN (SRGAN) [14] framework, denoted as Semi-SRGAN (SSRGAN). The primary objective of SSRGAN is to accurately restore the deteriorated segments within images. Also, Figure 1 shows an example of the output of our model. Moreover, leveraging the power of both the generator and discriminator components inherent to generative models, our approach is proficient in predicting the missing pixels with minimal loss.

II. Approach

A. Methods

In the context of deep learning, particularly in the domain of image inpainting, this study focuses on the training process of our deep learning model. A key component of this training involves deliberately introducing pixel corruption to the input images.

To execute this corruption procedure, we adopt a random and uniform pixel selection approach. Specifically, we randomly identify pixels within the image, ensuring a uniform distribution across the entire image canvas. Subsequently, we apply the chosen corruption technique to the selected pixels. These corrupted images are then utilized as inputs for our deep learning model.

B. Network architecture

Deep learning models can be effectively harnessed to fulfil our designated objectives. Within this investigation, we have leveraged a modified iteration of the (SRGAN) to

assess the reconstruction of missing pixels. Given the intricate structure and extensive parameterization inherent in the original SRGAN architecture, a tailored adaptation was executed to align with our specific demands, leading to the conception of the Semi Super-Resolution GAN (SSRGAN).

In the pursuit of enriching the fidelity of fake data, the employment of a generative model has been instrumental in generating real data representations from latent noise vectors. Furthermore, the predictive capabilities of GAN models are harnessed to yield precise estimations of image pixels. Within the domain of high-resolution images, the super-resolution approach capitalizes on pixel correlations to yield remarkably accurate forecasts for newly introduced pixels.

Moreover, within the ambit of this inquiry, the SSRGAN framework emerges as a pivotal tool, empowering us to minutely appraise pixel attributes and strive for optimal performance measured by the final metric of Normalized Mean Squared Error (NMSE).

The generative adversarial networks consist of two main parts that were named Generator (G) and Discriminator (D). The generator gives the input image a size of $(C \times H \times W)$ and the output size is the same as the input dimension.

On the other side, the discriminator is also like a referee that compares the output of the generator (\hat{H}_{SR}) with the real high-resolution channel (H_{SR}). Equation (1) shows the mechanism of the GAN that H_{SR} and H_{LR} denote the real high-resolution and low-resolution channels, respectively.

$$\min_G \max_D V(D, G) = \mathbb{E}_{H_{SR} \sim p_{train}(H_{SR})} [\log D(H_{SR})] + \dots \\ \mathbb{E}_{H_{LR} \sim p_G(H_{LR})} [\log(1 - D(G(H_{LR})))] \quad (1)$$

Figure 2 shows our SSRGAN model, with (a) representing the generator network and (b) the discriminator network. The generator comprises 6 convolutional blocks, where the convolutional layers in each block have a kernel size of 3 and a stride of 1, connected by residual links to enhance its performance. It culminates in a final convolutional layer with a kernel size of 9 and a stride of 4, matching the input size. Moreover, a convolutional layer was used with a kernel size of 9 and a stride of 1 at the beginning of the generator network.

To achieve high-resolution conversion, our SRGAN model utilizes the pixel shuffler technique. This technique is well-known for its effectiveness in super-resolution models, as it rearranges pixels within feature maps to enhance image resolution significantly. By incorporating this technique into our model, we successfully generated high-quality, finely-detailed images, resulting in an overall improvement in output fidelity. Importantly, the pixel shuffler layer within the generator employs an upscale factor (r) of 2.

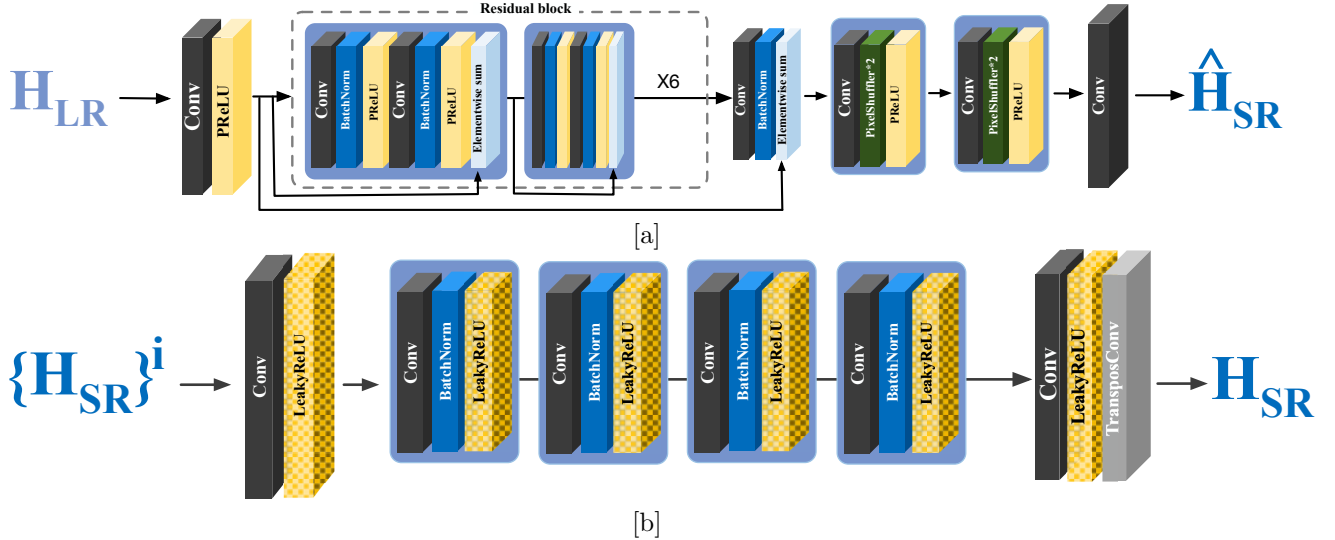


Fig. 2. The proposed Semi-Super Resolution GAN (SSRGAN) model for image inpainting. (a) The SSRGAN generator. (b) The discriminator for training the SSRGAN generator.

Our model's discriminator network differs from the original SRGAN in several key aspects. Instead of the original design, our model employs a discriminator network comprising four blocks. Each of these blocks handles an increasing number of channels, ranging from 64 to 512, with the number of images doubling at each successive block. We accomplished this by utilizing a transpose convolution operation with a kernel size of 4 and a stride of 4 for the final layer of our discriminator network.

C. Loss Function

Using pre-trained models on the ImageNet [15] dataset, the main SRGAN defined a specific loss function that was called VGG-loss. Accordingly, this method has more complexity and a longer training process. Therefore, we use MSE loss instead of VGG19 [16] loss for training our model. In addition, in the discriminator network because of the classification tasks, the authors of SRGAN used Binary Cross Entropy (BCE) loss, but due to our work, we replaced it with MSE loss.

The loss function for the discriminator defined in Equation (2) is that \mathcal{L}_F and \mathcal{L}_R represent the loss of fake generated data given to the discriminator and real data respectively.

$$\text{Loss}_D = \mathcal{L}_F + \mathcal{L}_R. \quad (2)$$

As shown in equation (3), for computing the \mathcal{L}_R we have to measure the MSE between the real high-resolution channel (H_{SR}) sent to the discriminator which we named D_R , and an ones matrix 1 that is minus by 0.1α . α here is a random uniform matrix with $H \times W$ dimension.

$$\mathcal{L}_R = \text{MSE}(D_R, 1 - 0.1\alpha). \quad (3)$$

Moreover, \hat{H}_{SR} sent to the discriminator and called it D_F . Although, \mathcal{L}_F shows the MSE between the D_F and a zero matrix (S_D) with the dimension of $H \times W$, so we will have this loss as follow:

$$\mathcal{L}_F = \text{MSE}(D_F, S_D). \quad (4)$$

To calculate the generator's loss in Equation (5), it comprises two components. The first component computes the MSE between the reconstructed image (\hat{H}_{SR}) and the original image (H_{SR}). In the second component, we compute the MSE between D_F and a one matrix (1).

$$\text{Loss}_G = \text{MSE}(\hat{H}_{SR}, H_{SR}) + 10^{-3}(\text{MSE}(D_F, 1)). \quad (5)$$

D. Dataset

In this study, our deep learning model was trained on a limited number of datasets. Consequently, we employed three distinct dataset types: Oxfordiiitpet [17], Caltec101 [18], and Flower102 [19]. It is important to emphasize that, in order to accommodate the computational demands of training on these datasets, we resized all images to dimensions of 128×128 . Further details regarding the datasets, including the number of datasets, are presented in Table I .

TABLE I
Detail of dataset

Dataset	Trainset	Testset
Oxfordiiitpet	3680	3669
Caltec101	7315	1829
Flower102	1020	6149

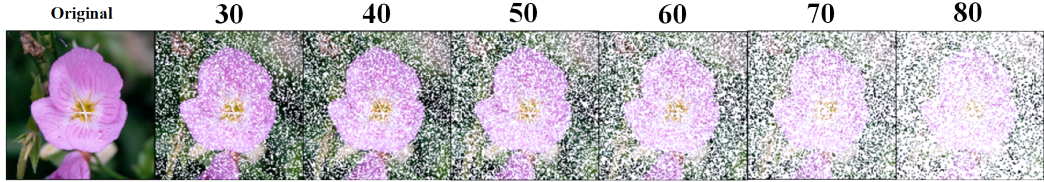


Fig. 3. A representation of levels pixel corruption from 30% to 80%

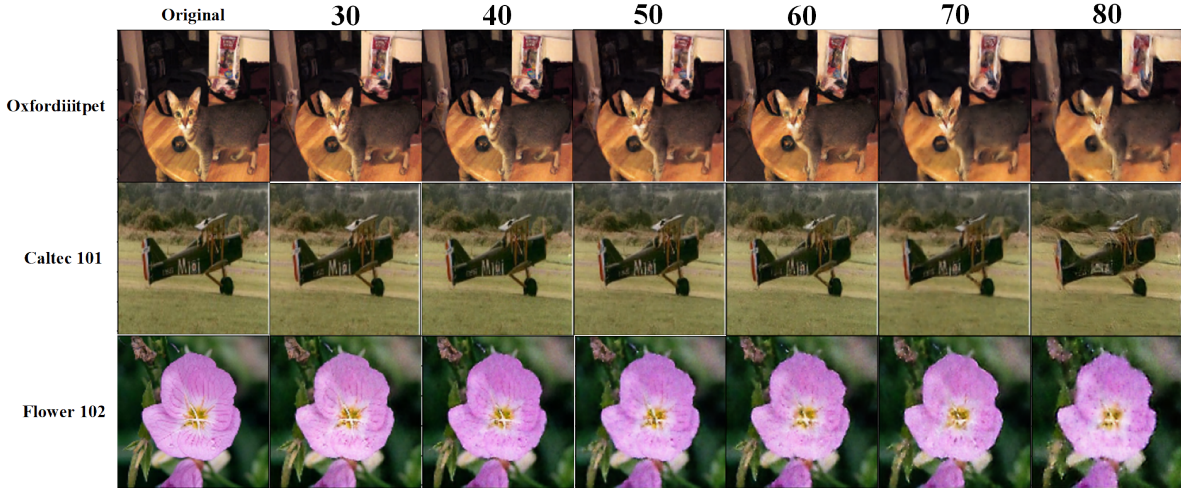


Fig. 4. The result of output images from Oxfordiiitpet, Caltec101, and Flower102 datasets on our SSRGAN for each degree of eliminated pixels.

III. Results

After training our model on three distinct datasets, we initiated the evaluation process on test data. It is imperative to underscore that we employed the Normalized Mean Square Error (NMSE), as denoted in Equation 6, as the primary performance metric during the simulations. This metric was utilized to quantify the extent to which the model's output resembled the original image.

$$\text{NMSE} = \mathbb{E}_{H_{\text{SR}}} \left\{ \frac{\|H_{\text{SR}} - \hat{H}_{\text{SR}}\|_F^2}{\|H_{\text{SR}}\|_F^2} \right\}. \quad (6)$$

In addition to NMSE, we also report the Peak Signal-to-Noise Ratio (PSNR), a widely used evaluation metric in image inpainting and image restoration tasks. PSNR quantifies the reconstruction fidelity by comparing the mean squared error (MSE) between the reconstructed and ground-truth images to the maximum possible pixel intensity, and is defined as:

$$\text{PSNR} = 10 \log_{10} \left(\frac{\text{MAX}^2}{\text{MSE}} \right). \quad (7)$$

Since NMSE is derived from the same squared reconstruction error, PSNR, as defined in (7), can be directly related to NMSE through the mean squared error (MSE) term. While NMSE quantifies the normalized energy of

the reconstruction error, PSNR expresses the same error on a logarithmic scale relative to the signal dynamic range. Consequently, the inclusion of PSNR provides a complementary evaluation perspective and facilitates direct comparison with existing image inpainting and super-resolution methods reported in the literature.

Table II presents a quantitative comparison between NMSE and PSNR values obtained at the final training epoch for all evaluated datasets. The reported results correspond to a pixel corruption level of 50%, illustrating the inverse relationship between the two metrics, where lower NMSE values consistently result in higher PSNR.

TABLE II
PSNR and NMSE

Dataset	PSNR	NMSE
Oxfordiiitpet	20.36	0.0092
Caltec101	21.14	0.0077
Flower102	17.99	0.0159

To train our model, we employed an NVIDIA V100 GPU for 100 epochs. Specifically, for our SSRGAN training, we configured a batch size of 64 and utilized the Adam optimizer [20] for both the generators and discriminators. Furthermore, we set the values of β_1 and β_2 for the Adam optimizer to 0.9 and 0.999, respectively. To enhance

training stability, a learning rate scheduler was employed, reducing the learning rate by a factor of 0.5 every 25 epochs. Additionally, the initial learning rate was set to 0.0002.

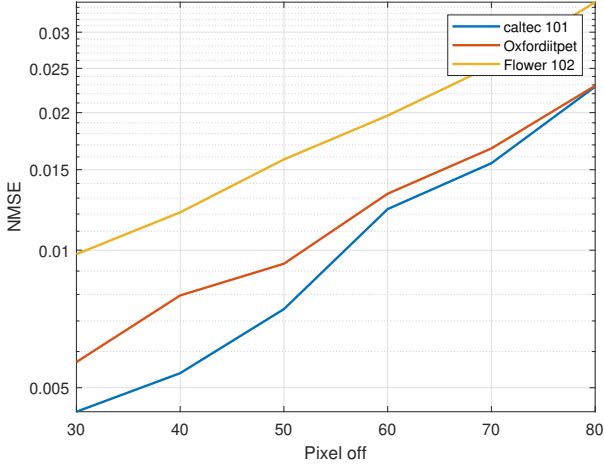


Fig. 5. Changes of NMSE by increasing the level of pixels off for three datasets.

In evaluating our model, as illustrated in Figure 3, we subjected each dataset to training under six distinct levels of pixel corruption, ranging from 30% to 80%. To elaborate, we initiated the training process by randomly corrupting 30% of all image pixels and subsequently training the model. This procedure was repeated for varying degrees of pixel corruption, enabling us to assess the model's robustness. Figure 4 provides a visual representation of the model's evaluation across all three datasets. Ultimately, we quantified the disparity between the generated images and their corresponding ground truth using the Normalized Mean Square Error (NMSE).

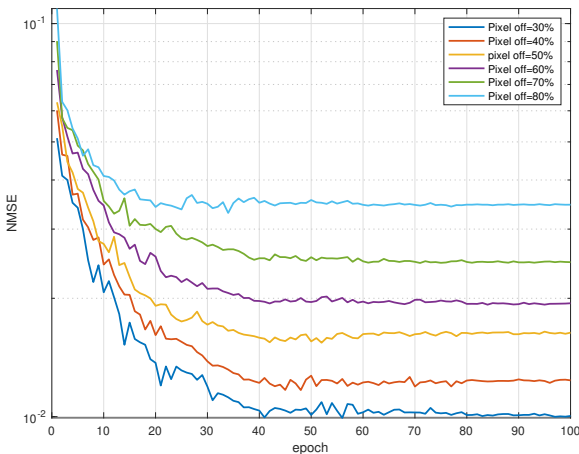


Fig. 6. Changes of NMSE for each epoch on with different level of pixels off

Whatsoever, as obtained in Figure 5 we measure the NMSE metric on each dataset for all levels of pixel corruption. As it is obvious, due to the higher number of testing data than the training data for the Flower102, the amount of NMSE for this dataset is significantly higher than the others. Also, by increasing the levels of pixel corruption, the NMSE increased.

Furthermore, Figure 6 illustrates the progression of NMSE values across epochs at various levels of pixel corruption on the flower102 dataset. Notably, it is evident that NMSE values increase as the percentage of corrupted pixels rises.

IV. Conclusion

In this paper, we applied a generative model to restore missing or corrupted pixels in image inpainting tasks. Additionally, we introduced a variant of SRGAN called Semi Super-Resolution GAN (SSRGAN) with reduced complexity and fewer parameters for the purpose of pixel reconstruction. Furthermore, we conducted training and testing using three distinct datasets and introduced Normalize-MSE (NMSE) as a metric to assess the similarity between the reconstructed and original images.

References

- [1] Q. Xiao, K. Lee, S. A. Mokhtar, I. Ismail, A. L. b. M. Pauzi, Q. Zhang, and P. Y. Lim, "Deep learning-based ecg arrhythmia classification: A systematic review," *Applied Sciences*, vol. 13, no. 8, p. 4964, 2023.
- [2] M. Momen-Tayefeh, M. Momen-Tayefeh, F. Z. Hasheminasab, and S. A. G. Ghahramani, "Snr gan: The semi noise reduction gan for image denoising," in 2024 20th CSI International Symposium on Artificial Intelligence and Signal Processing (AISP), 2024, pp. 1–5.
- [3] M. M. Tayefeh, S. A. G. Ghahramani, and A. M. A. Hemmatyar, "Advancing brain tumor detection via vircnn: A fusion of vision transformers and faster r-cnn," in 2025 15th International Conference on Computer and Knowledge Engineering (ICCKE). IEEE, 2025, pp. 1–6.
- [4] M. Momen-Tayefeh, M. Momen-Tayefeh, S. A. G. Ghahramani, and A. M. A. Hemmatyar, "Channel estimation for massive mimo systems aided by intelligent reflecting surface using semi-super resolution gan," *Signal Processing*, p. 109710, 2024.
- [5] M. Momen-Tayefeh, M. Momen-Tayefeh, and M. Sabbaghian, "Multi-block attention for efficient channel estimation in irs-assisted mmwave mimo," *IEEE Transactions on Communications*, 2025.
- [6] C. Barnes, E. Shechtman, A. Finkelstein, and D. B. Goldman, "Patchmatch: A randomized correspondence algorithm for structural image editing," *ACM Trans. Graph.*, vol. 28, no. 3, p. 24, 2009.
- [7] J. Hays and A. A. Efros, "Scene completion using millions of photographs," *ACM Transactions on Graphics (ToG)*, vol. 26, no. 3, pp. 4–es, 2007.
- [8] J. Yu, Z. Lin, J. Yang, X. Shen, X. Lu, and T. S. Huang, "Free-form image inpainting with gated convolution," in *Proceedings of the IEEE/CVF international conference on computer vision*, 2019, pp. 4471–4480.
- [9] G. Liu, F. A. Reda, K. J. Shih, T.-C. Wang, A. Tao, and B. Catanzaro, "Image inpainting for irregular holes using partial convolutions," in *Proceedings of the European conference on computer vision (ECCV)*, 2018, pp. 85–100.
- [10] D. Pathak, P. Krahenbuhl, J. Donahue, T. Darrell, and A. A. Efros, "Context encoders: Feature learning by inpainting," in *Proceedings of the IEEE conference on computer vision and pattern recognition*, 2016, pp. 2536–2544.

- [11] U. Demir and G. Unal, "Patch-based image inpainting with generative adversarial networks," arXiv preprint arXiv:1803.07422, 2018.
- [12] J. Yu, Z. Lin, J. Yang, X. Shen, X. Lu, and T. S. Huang, "Generative image inpainting with contextual attention," in Proceedings of the IEEE conference on computer vision and pattern recognition, 2018, pp. 5505–5514.
- [13] C. Yang, X. Lu, Z. Lin, E. Shechtman, O. Wang, and H. Li, "High-resolution image inpainting using multi-scale neural patch synthesis," in Proceedings of the IEEE conference on computer vision and pattern recognition, 2017, pp. 6721–6729.
- [14] C. Ledig, L. Theis, F. Huszár, J. Caballero, A. Cunningham, A. Acosta, A. Aitken, A. Tejani, J. Totz, Z. Wang et al., "Photo-realistic single image super-resolution using a generative adversarial network," in Proceedings of the IEEE conference on computer vision and pattern recognition, 2017, pp. 4681–4690.
- [15] J. Deng, W. Dong, R. Socher, L.-J. Li, K. Li, and L. Fei-Fei, "Imagenet: A large-scale hierarchical image database," 2009 IEEE conference on computer vision and pattern recognition, pp. 248–255, 2009.
- [16] K. Simonyan and A. Zisserman, "Very deep convolutional networks for large-scale image recognition," arXiv preprint arXiv:1409.1556, 2014.
- [17] O. M. Parkhi, A. Vedaldi, A. Zisserman, and C. Jawahar, "Cats and dogs," in 2012 IEEE conference on computer vision and pattern recognition. IEEE, 2012, pp. 3498–3505.
- [18] L. Fei-Fei, R. Fergus, and P. Perona, "Learning generative visual models from few training examples: An incremental bayesian approach tested on 101 object categories," in 2004 conference on computer vision and pattern recognition workshop. IEEE, 2004, pp. 178–178.
- [19] M.-E. Nilsback and A. Zisserman, "Automated flower classification over a large number of classes," in 2008 Sixth Indian conference on computer vision, graphics & image processing. IEEE, 2008, pp. 722–729.
- [20] D. P. Kingma and J. Ba, "Adam: A method for stochastic optimization," arXiv preprint arXiv:1412.6980, 2014.